# Journal Pre-proofs


Regular paper

Cost-Efficient Surrogate Modeling of High-Frequency Structures Using Nested Kriging with Automated Adjustment of Model Domain Lateral Dimensions

Anna Pietrenko-Dabrowska, Slawomir Koziel

PII: S1434-8411(20)30548-3
DOI: https://doi.org/10.1016/j.aeue.2020.153224
Reference: AEUE 153224

To appear in: *International Journal of Electronics and Communications*

Received Date: 6 March 2020
Accepted Date: 19 April 2020

Please cite this article as: A. Pietrenko-Dabrowska, S. Koziel, Cost-Efficient Surrogate Modeling of High-Frequency Structures Using Nested Kriging with Automated Adjustment of Model Domain Lateral Dimensions, *International Journal of Electronics and Communications* (2020), doi: https://doi.org/10.1016/j.aeue.2020.153224

# Cost-Efficient Surrogate Modeling of High-Frequency Structures Using Nested Kriging with Automated Adjustment of Model Domain Lateral Dimensions

Anna Pietrenko-Dabrowska[1] and Slawomir Koziel[1,2]

[1] Faculty of Electronics, Telecommunications and Informatics, Gdansk University of Technology, 80-233 Gdansk, Poland, anna.dabrowska@pg.edu.pl

[2] Engineering Optimization & Modeling Center, Reykjavik University, 101 Reykjavik, Iceland, koziel@ru.is,

Corresponding author: anna.dabrowska@pg.edu.pl

**Keywords:** High-frequency modeling; surrogate modeling; nested kriging; domain confinement; simulation-driven design.

**Abstract**

Surrogate models are becoming popular tools of choice in mitigating issues related to the excessive cost of electromagnetic (EM)-driven design of high-frequency structures. Among available techniques, approximation modeling is by far the most popular due to its versatility. In particular, the surrogates are exclusively based on the sampled simulation data with no need to involve engineering insight or problem-specific knowledge. Notwithstanding, a typically high nonlinearity of system outputs and the curse of dimensionality limit the applicability of conventional methods to relatively simple structures described by a few parameters within narrow ranges thereof. A recently reported nested kriging alleviates these difficulties from the perspective of an appropriate definition of the model domain. By focusing the modeling process on the region containing design that are optimized for the selected performance figures, it enables the construction of reliable surrogates over wide ranges of geometry/material parameters and operating conditions, both at a practically acceptable computational cost. The relative model domain thickness (i.e., its lateral-to-tangential size), determines the trade-off between the surrogate region of coverage and its predictive power, the former being essential for practical applications of the model, especially design optimization. This paper proposes a simple and computationally efficient procedure for automatic selection of the thickness parameter, which, in the original version of the method, was to be selected by the user. The importance of this aspect of the modeling process and the benefits of the proposed approach are demonstrated using a dual-band dipole antenna and miniaturized microstrip coupler.

## 1. Introduction

The design of modern high-frequency structures, including microwave, antenna, and integrated photonic components, heavily relies on full-wave electromagnetic (EM) simulation tools. The employment of EM analysis is imperative to account for the effects and phenomena that cannot be reliably quantified using simpler means such as analytical or equivalent network models. Examples include EM cross-coupling in tightly arranged layouts of miniaturized microstrip circuits (filters [1], couplers [2]), mutual coupling in antenna arrays [3], the effects of connectors on electrical characteristics [4], distortion of antenna radiation patterns due to housing or radomes [5], characterization of wearable antennas under bending [6], as well as multi-physics evaluation (e.g., variations of high-power filter dimensions due to heating and the effects on return loss and transmission responses [7]). Unfortunately, full-wave analysis often incurs considerable computational expenditures. Typically, this is not an issue for design verification; however, repetitive simulations required by routinely executed tasks such as parameter tuning may turn prohibitive.

Several classes of methods are available to mitigate the aforementioned cost. One posadjoint senistivitysibility is the development of numerically efficient algorithms, both intrusive (e.g., adjoint sensitivities [8], [9] and their application to speed up gradient-based search procedures [10]) and non-intrusive (e.g., gradient search algorithms with sparse sensitivity updates [11], [12]). Another option is the utilization of fast surrogate models. In the context of local design optimization, the surrogates are normally constructed in the vicinity of the optimization path and can be either data-driven (polynomial regression [13], kriging [14], neural networks [15], polynomial chaos expansion [16]) or physics-based [17]. The latter is obtained from the underlying low-fidelity models, e.g., equivalent networks in the case of microstrip circuits [17], or coarse-mesh EM simulations in the case of antennas [18]. Representative optimization techniques include space mapping [19], feature-based

optimization [20], and various response correction methods [21]. In the context of global optimization, machine learning techniques are often employed [22], [23], as well as data-driven surrogates in combination with sequential sampling methods [24]. Other types of simulation-driven design tasks can be accelerated using dedicated types of surrogates, with the representative example of polynomial chaos expansion models used for statistical analysis and robust design [25], [26].

The overall replacement of expensive EM simulations by fast surrogates is a conceptually attractive option. It potentially enables low-cost execution of various simulation-based procedures, including parametric optimization. For this purpose, data-driven models seem to be especially suitable due to their versatility and easy access through various toolboxes, often Matlab based (e.g., [27], [28]). Popular approximation techniques include radial basis functions [29], kriging [30], Gaussian process regression [31], support vector regression [32], or neural networks [33]. Notwithstanding, modeling of high-frequency structures is a challenging endeavor due to several reasons: (i) considerable nonlinearity of the system responses, typically being the functions of frequency (e.g., return loss, transmission coefficient, gain, axial ratio, etc.), (ii) the need for constructing the models over wide ranges of the system parameters and its operating conditions, (iii) the curse of dimensionality, i.e., a rapid increase of the number of training data samples required to build a reliable model as a function of the number of system parameters. The second reason is dictated by the design utility of the surrogate, whereas the last one is a common problem for all sorts of data-driven models. Methods such as high dimensional model representation (HDMR) [34], orthogonal matching pursuit (OMP) [35], least-angle regression [36], or variable-fidelity approaches (co-kriging [37], Bayesian model fusion [38]) can be used to alleviate some of the mentioned issues under certain circumstances (e.g., the existence of small subsets of dominant basis functions for OMP, or availability of well-correlated low-fidelity models for co-kriging [37]).

Recently, performance-driven (or constrained) modeling has been fostered as a way of constructing reliable surrogates at practically acceptable computational costs [39]-[41]. The major concept is a confinement of the model domain to a region containing designs that are nearly optimum with respect to the figures of interest relevant to the design problem at hand (operating frequencies, bandwidth, power split ratio, etc.). The domain is defined using a set of reference designs pre-optimized for selected performance figure vectors [39]; the details of analytical formulation vary between the methods.

Among the reported techniques, the nested kriging framework [41] seems to be the most attractive because it permits handling several performance figures, allows for the arbitrary allocation of the reference designs, and incorporates straightforward mechanisms for uniform training data sampling and model optimization [41]. The technique employs two kriging interpolation metamodels, the first-level one to establish the domain, and the second-level model being the actual surrogate. However, the critical control parameter determining the domain thickness (i.e., the ratio between the lateral and tangential size of it) remains to be selected by the user. This parameter determines the domain volume, therefore directly affects (given the training data set) the predictive power of the surrogate [41]. At the same time, it also determines whether the surrogate accounts for all (or part) of the designs being optimum with respect to the selected figures of interest. The latter is necessary to make the model suitable for design purposes. Unfortunately, the nested kriging formalism does not provide any indication concerning the recommended value of the thickness parameter. This paper proposes a simple and computationally efficient method for setting it up in an automated manner. Our approach is based on estimating the domain thickness required for the surrogate to find the optimum design throughout the objective space. The estimation is carried out at the locations corresponding to the lowest accuracy of the first-level surrogate (i.e., worst-case scenarios), and then averaged over the entire space. The relevance of our methodology is validated through

consistency comparisons with the actual nested-kriging surrogates constructed for a range of thickness values. The verification experiments carried out for a dual-band dipole antenna, and a miniaturize rat-race coupler corroborate the reliability of the recommendations provided by the proposed approach.

## 2. Surrogate Modeling by Nested Kriging

This section outlines the concept and formulation of the nested kriging modelling framework. The proposed automated adjustment of the domain thickness parameter being the main topic of this work will be discussed in Section 3.

### 2.1. Reference Designs and First-Level Surrogate

A conventional way of defining the surrogate model domain is through the lower and upper bounds for design variables. Interval domains are convenient to handle especially from the point of view of the design of experiments (training data sample allocation) and model optimization. Notwithstanding, the vast majority of the domain contains designs that are of poor quality. This is due to correlations between the optimum or nearly optimum parameter sets, corresponding to, e.g., the structure re-designed for various operating frequencies or bandwidths [41]. Performance-driven (or constrained) modeling [39] restricts the surrogate construction process to the region that contains high-quality designs with respect to relevant performance figures. The volume of such a region is dramatically smaller than the box-constrained original domain. This translates into computational savings in terms of training data acquisition [40]. The nested kriging framework is a recent methodology following this approach [41]. The model domain is defined using the set of reference designs and the first-level model as outlined below.

Let $\boldsymbol{x} = [x_1 \ldots x_n]^T$ be the vector of parameters of the high-frequency structure of interest. The (original) parameter space $X$ is defined by the lower and upper bounds $\boldsymbol{l} = [l_1 \ldots, l_n]^T$ and

$\boldsymbol{u} = [u_1 \ldots, u_n]^T$, so that $l_k \le x_k \le u_k$ for $k = 1, \ldots, n$. Let $f_k$, $k = 1, \ldots, N$, denote the figures of interest pertinent to the design task (e.g., operating frequencies for a multi-band antenna or power split ratio for a coupler). The objective space $F$ is defined by the ranges $f_{k.\min} \le f_k^{(j)} \le f_{k.\max}$, $k = 1, \ldots, N$. This is the intended region of validity for the surrogate.

Given the objective vector $\boldsymbol{f} \in F$, the optimum design corresponding to $\boldsymbol{f}$ is understood as the solution to the problem

$$\boldsymbol{x}^* = U_F(\boldsymbol{f}) = \arg\min_{\boldsymbol{x}} U(\boldsymbol{x}, \boldsymbol{f}) \tag{1}$$

where $U$ is the scalar merit function quantifying the design utility. $U_F(F)$ represents all designs that are optimum in the sense of (1) for all $\boldsymbol{f} \in F$. The surrogate model domain is to be established in the vicinity of this set.

According to [41], $U_F(F)$ can be approximated using the reference designs $\boldsymbol{x}^{(j)} = [x_1^{(j)} \ldots x_n^{(j)}]^T$ $j = 1, \ldots, p$, optimized w.r.t. the performance vectors $\boldsymbol{f}^{(j)} = [f_1^{(j)} \ldots f_N^{(j)}]$ uniformly distributed within $F$; $\boldsymbol{x}^{(j)}$ may be available from the previous design work on the same structure or obtained specifically for surrogate model construction. The data set $\{\boldsymbol{f}^{(j)}, \boldsymbol{x}^{(j)}\}$ is used to identify the first-level surrogate model $\boldsymbol{s}_I(\boldsymbol{f})$ that maps $F$ into the parameter space $X$. It is implemented using kriging interpolation [30]. The image of the objective space through $\boldsymbol{s}_I$, $\boldsymbol{s}_I(F) \subset X$, is the approximation of $U_F(F)$. A graphical illustration of the concepts introduced in this section can be found in Fig. 1.

### 2.2. Model Domain. Second-Level Surrogate

As illustrated in Fig. 1, the manifolds $U_F(F)$ and $\boldsymbol{s}_I(F)$ coincide at all reference designs $\boldsymbol{x}^{(j)}$. However, the number of such designs is normally small so the accuracy of $\boldsymbol{s}_I(F)$ is limited. To ensure that the model domain contains the entire $U_F(F)$, an enlargement of $\boldsymbol{s}_I(F)$ is necessary. Within the nested kriging framework, it is realized through an orthogonal extension of $\boldsymbol{s}_I(F)$ towards its normal vectors.

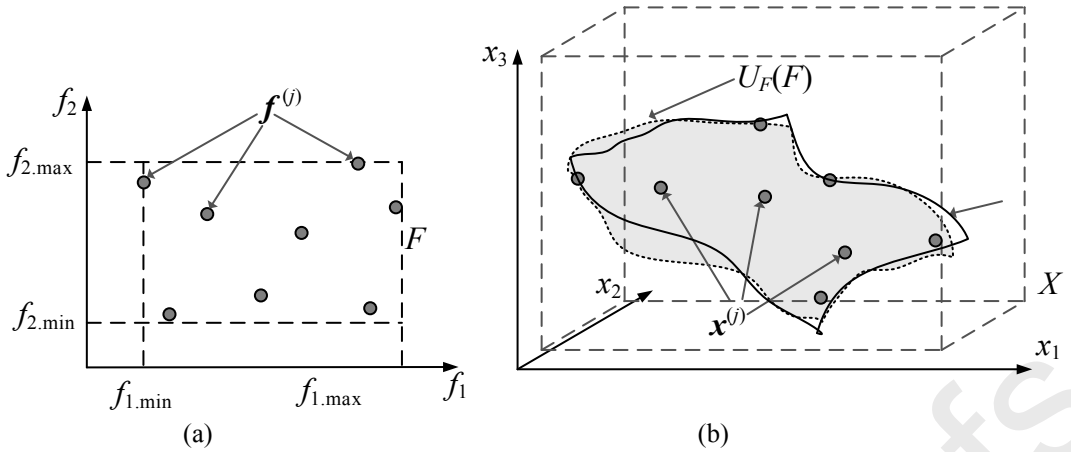


Fig. 1. Graphical illustration of the concepts considered in Section 2.1: (a) objective space $F$ (here, shown for two performance figures), (b) parameter space $X$ (here, three-dimensional), the reference designs, the optimum design manifold $U_F(F)$, and the first-level surrogate image $\boldsymbol{s}_I(F)$. Because the reference designs $\boldsymbol{x}^{(j)}$ are optimal in the sense of (1), the manifolds $U_F(F)$ and $\boldsymbol{s}_I(F)$ coincide at all $\boldsymbol{x}^{(j)}$.

The following notation is utilized:

- $\{\boldsymbol{v}_n^{(k)}(\boldsymbol{f})\}$, $k = 1, \ldots, n - N$ - an orthonormal basis of vectors normal to $\boldsymbol{s}_I(F)$ at $\boldsymbol{f}$,
- $\boldsymbol{x}_{\max} = \max\{\boldsymbol{x}^{(k)}, k = 1, \ldots, p\}$,
- $\boldsymbol{x}_{\min} = \min\{\boldsymbol{x}^{(k)}, k = 1, \ldots, p\}$,
- $\boldsymbol{x}_d = \boldsymbol{x}_{\max} - \boldsymbol{x}_{\min}$ (parameter variations within $\boldsymbol{s}_I(F)$)

Using these, the extension coefficients can be defined as

$$\boldsymbol{\alpha}(\boldsymbol{f}) = [\alpha_1(\boldsymbol{f}) \ldots \alpha_{n-N}(\boldsymbol{f})]^T = 0.5T\left[|\,\boldsymbol{x}_d \boldsymbol{v}_n^{(1)}(\boldsymbol{f})\,| \;\ldots\; |\,\boldsymbol{x}_d \boldsymbol{v}_n^{(n-N)}(\boldsymbol{f})\,|\right]^T \tag{2}$$

where $T$ is a user-defined thickness parameter. The coefficients $\alpha_k$ determine the boundaries of the surrogate model domain $X_S$, which is located between the two manifolds:

$$M_{\pm} = \left\{\boldsymbol{x} \in X : \boldsymbol{x} = \boldsymbol{s}_I(\boldsymbol{f}) \pm \sum\nolimits_{k=1}^{n-N} \alpha_k(\boldsymbol{f}) \boldsymbol{v}_n^{(k)}(\boldsymbol{f})\right\} \tag{3}$$

The formal definition of $X_S$ takes the form of

$$X_S = \left\{ \begin{array}{c} \boldsymbol{x} = \boldsymbol{s}_I(\boldsymbol{f}) + \sum\limits_{k=1}^{n-N} \lambda_k \alpha_k(\boldsymbol{f}) \boldsymbol{v}_n^{(k)}(\boldsymbol{f}) : \boldsymbol{f} \in F, \\ -1 \le \lambda_k \le 1, k = 1, \ldots, n-N \end{array} \right\} \tag{4}$$

Figure 2 provides a graphical illustration of the manifolds $M_+$ and $M_-$, as well as the domain $X_S$. The second-level (i.e., the actual) surrogate is also a kriging interpolation model

rendered in $X_S$, using $\{\boldsymbol{x}_B^{(k)},\boldsymbol{R}(\boldsymbol{x}_B^{(k)})\}_{k = 1, \ldots, NB}$, as the training set, where $\boldsymbol{x}_B^{(k)}$ are the training samples uniformly allocated in the domain, whereas $\boldsymbol{R}$ is the EM-simulation model of the high-frequency structure of interest. The details concerning the sampling procedure can be found in [41].

The major computational benefit of the nested kriging technique is that the volume of the domain $X_S$ is significantly smaller than that of the original parameter space $X$. This directly translates into a considerably smaller number of training data samples required to establish a reliable model (or, equivalently, the improved predictive power of the surrogate given the same training data set size). Furthermore, the surrogate can be constructed over wide ranges of the system parameters and its operating conditions. The advantages of the technique are especially pronounced in higher-dimensional spaces where conventional approach (i.e., modeling within the box-constrained domain $X$) is computationally infeasible.

## 3. Automated Adjustment of Domain Thickness

This section describes the proposed procedure for automated a priori determination of the thickness parameter $T$, which results in a possibly small volume of the surrogate model domain while ensuring that the majority of the optimum design manifold $U_F(F)$ is contained therein. A numerical verification of the method will be discussed in Section 4.

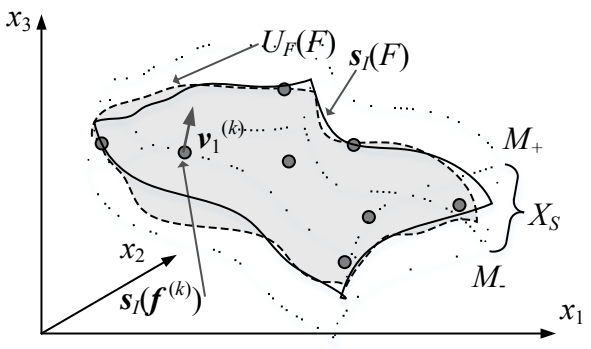


Fig. 2. The image $\boldsymbol{s}_I(F)$ of the first-level surrogate model and the normal vector $\boldsymbol{v}_1^{(k)}$ at $\boldsymbol{f}^{(k)}$; the manifolds $M_-$ and $M_+$ and the surrogate model domain $X_S$ defined as the orthogonal extension of $\boldsymbol{s}_I(F)$.

### 3.1. Domain Thickness: Importance and Selection Criteria.

As explained in Section 2, the nested kriging framework formulation only includes one control parameter, which is the domain thickness coefficient $T$. The modeling procedure does not give any indication about a suitable value of this parameter, which is otherwise critical from the point of view of the model accuracy, the cost of training data acquisition, and the model design utility [41]. On the one hand, decreasing $T$ results in a significant reduction of the domain volume, by a factor $(T_1/T_2)^{n-N}$, where $T_1$ and $T_2$ are previous and the new thickness parameter values, respectively. For example, diminishing $T$ by 50 percent when operating in 10-dimensional parameter space ($n = 10$) and two-dimensional objective space ($N = 2$), reduces the model domain volume by almost three orders of magnitude, which has a profound effect on the model accuracy. On the other hand, reducing $T$ may lead to leaving a certain part (or even a majority) of the optimum design manifold $U_F(F)$ out of $X_S$. The consequence is reduced design usefulness of the surrogate because the exact optimum is unreachable for some regions of the objective space. Figure 3 provides a graphical illustration.

For demonstration examples reported in the literature [41], [42], $T$ was selected in the range between 0.05 and 0.15 with no further justification. Available numerical studies confirm the clear dependence of the model predictive power on the value of $T$.

Here, our objective is to develop a methodology for a priori estimation of the suitable value of the thickness parameter. The procedure should meet the following criteria being a combination of practical utility and computational efficiency:

- The estimation process should not entail excessive computational expenses; consequently, the employment of already available information (specifically, the reference designs) is preferred;
- The obtained $T$-value should ensure that the model domain $X_S$ contains a majority of the optimum design manifold $U_F(F)$;

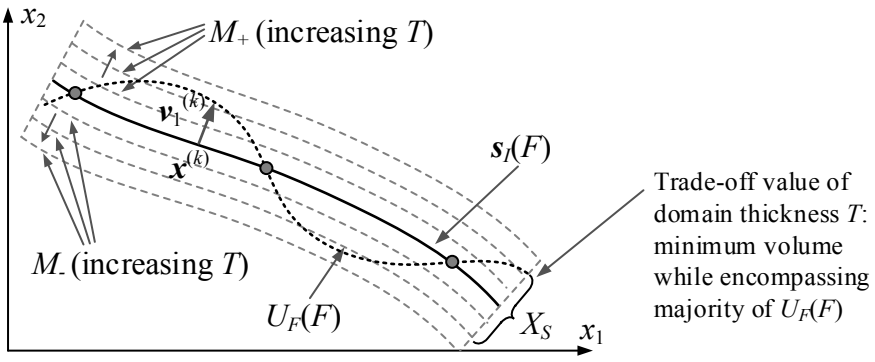


Fig. 3. Graphical illustration of the meaning of the thickness parameter $T$, for clarity, explained using two-dimensional parameter space. Increasing $T$ enlarges the model domain which allows for encapsulating the optimum design manifold $U_F(F)$. At the same time, a larger domain requires more training samples to render reliable surrogate. The desired trade-off is to find the minimum value of $T$ that still permits the incorporation of the majority of $U_F(F)$.

- While retaining the property above, the thickness parameter should be of possibly minimum value.

### 3.2. Automated Determination of Thickness Parameter

The proposed estimation procedure is based on emulating surrogate model optimization; specifically, the behavior of the objective function value $U$ for the optimization runs executed over a range of thickness parameter values. Reaching saturation of $U$ indicates that the model domain contains the manifold $U_F(F)$.

At this stage of the process, the second-level surrogate does not exist: finding a proper value of the thickness parameter is a prerequisite for further allocation of the training data and model identification. Therefore, the optimization as mentioned above is carried out using the linear (first-order Taylor) model of the system responses of the form

$$\boldsymbol{L}(\boldsymbol{z}) = \boldsymbol{R}(\boldsymbol{x}) + \boldsymbol{J}_R(\boldsymbol{x})(\boldsymbol{z} - \boldsymbol{x}) \tag{5}$$

set up at $\boldsymbol{x} \in \boldsymbol{s}_I(F)$. The model (5) requires the Jacobian matrix $\boldsymbol{J}_R$, here, estimated using finite differentiation. Because this entails $n$ additional EM simulations, the number of points $\boldsymbol{x}$ involved in the procedure is necessarily small. Consequently, their locations are of importance

and should correspond to those regions of the objective space where the discrepancy between $\boldsymbol{s}_I(F)$ and $U_F(F)$ is the largest. Although $U_F(F)$ is not known, it is expected that $\|\boldsymbol{s}_I(F) - U_F(F)\|$ is maximized between the reference designs (cf. Fig. 3). Having this in mind, the points $\boldsymbol{x}_T^{(j)}$ for thickness parameter determination are selected as the centers of the simplexes $S^{(j)}$ obtained by the triangulation of the reference designs. In this work, to avoid degenerated simplexes, Delaunay triangulation is employed [43]. Figure 4 shows a graphical illustration for two-dimensional objective space and three-dimensional parameter space.

Let $\boldsymbol{b} = [b_1 \ldots b_{n-N}]^T$ be a vector of coefficients such that $-1 \le b_k \le 1$, $k = 1, \ldots, n - N$, and let $\boldsymbol{f} \in F$. For a given the thickness parameter $T$ and vector $\boldsymbol{x}_T^{(j)} = \boldsymbol{s}_I(\boldsymbol{f}_T^{(j)})$, $j = 1, \ldots, N_S$ (here, $N_S$ is the number of simplexes $S^{(j)}$) the extension coefficients $a_k(\boldsymbol{f}_T^{(j)})$ are defined using (2). Consider the following minimization problem

$$E_j(T) = \min_{\boldsymbol{b},\boldsymbol{f}} U_R\left(\boldsymbol{L}^{(j)}\left(\boldsymbol{s}_I(\boldsymbol{f}) + \sum_{k=1}^{n-N} b_k a_k(\boldsymbol{f}_T^{(j)})\boldsymbol{v}_n^{(k)}(\boldsymbol{f}_T^{(j)})\right), \boldsymbol{f}_T^{(j)}\right) \tag{6}$$

with the starting point being $\boldsymbol{b} = [0 \ \ldots \ 0]^T$ and $\boldsymbol{f} = \boldsymbol{f}_T^{(j)}$, and $U_R$ being the merit function equivalent to $U$ but with explicit dependence on the system response $\boldsymbol{R}$, i.e., $U_R(\boldsymbol{R}(\boldsymbol{x}),\boldsymbol{f}) = U(\boldsymbol{x},\boldsymbol{f})$. Note that $\left[\boldsymbol{s}_I(\boldsymbol{f}) + \sum_{k=1}^{n-N} b_k a_k(\boldsymbol{f}_T^{(j)})\boldsymbol{v}_n^{(k)}(\boldsymbol{f}_T^{(j)})\right] - \boldsymbol{s}_I(\boldsymbol{f}_T^{(j)})$ represents a deviation from the starting point $\boldsymbol{x}_T^{(j)} = \boldsymbol{s}_I(\boldsymbol{f}_T^{(j)})$, with $\boldsymbol{s}_I(\boldsymbol{f}) - \boldsymbol{s}_I(\boldsymbol{f}_T^{(j)})$ and $\sum_{k=1}^{n-N} b_k a_k(\boldsymbol{f}_T^{(j)})\boldsymbol{v}_n^{(k)}(\boldsymbol{f}_T^{(j)})$ being tangential shift (i.e., along the manifold $\boldsymbol{s}_I(F)$) and orthogonal shift (i.e., towards the normal vectors $\boldsymbol{v}_n^{(k)}$), respectively. The linear model $\boldsymbol{L}^{(j)}$ is of the form (5), established at $\boldsymbol{x}_T^{(j)}$.

Let $T_1 = 0 < T_2 < \ldots < T_{NT}$, be a sequence of thickness parameters such that $T_{NT}$ is sufficiently large to ensure that the entire $U_F(F) \subset X_S$ for $X_S$ defined using $T_{NT}$ (in practice, using $T_{NT} = 0.2$ or so is sufficient in most practical cases). The sequence $E_j(T_k)$ obtained using (6) will be, therefore, decreasing and converging to $E_j(T_{NT})$. Consider the normalized sequences

$$E_{N.k}^{(j)} = \frac{E_j(T_k) - \min\{k : E_j(T_k)\}}{\max\{k : E_j(T_k)\} - \min\{k : E_j(T_k)\}} \tag{7}$$

and their average over $j = 1, \ldots, N_S$

$$E_{aver.k} = \frac{1}{N_S}\sum_{j=1}^{N_S} E_{N.k}^{(j)} \tag{8}$$

The recommended value of the thickness parameter, $T_{th}$, is assigned as the one corresponding to the average value of the normalized objective equal to the threshold level $E_{th}$. In this work, we use $E_{th} = 0.25$ as a trade-off between the surrogate domain volume and the coverage of the manifold $U_F(F)$. Figure 5 provides a graphical illustration of the introduced concepts.

The above procedure employs several approximations; in particular, it utilizes the linear model of the system responses, as well as information gathered from a limited number of points across the parameter space. At the same time, it is computationally efficient because it only required $N_S(n + 1) \approx p(n + 1)$ EM simulations (the number of simplexes $S^{(i)}$ is normally close to the number $p$ of the reference designs).

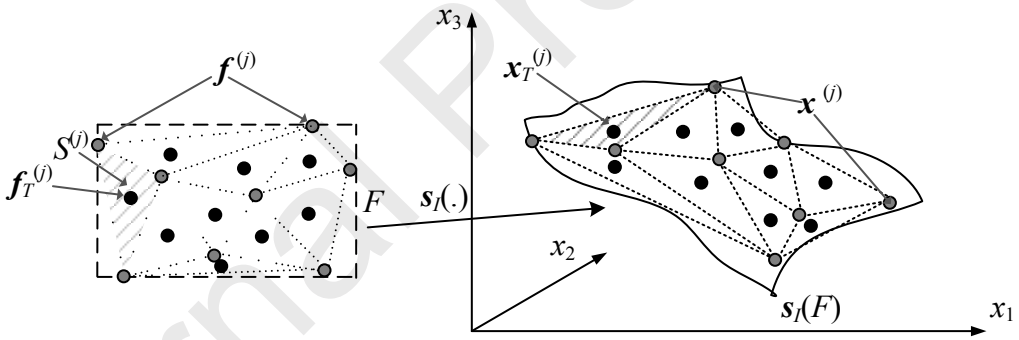


Fig. 4. Triangulation of the reference designs performed in the objective space. The centers $\boldsymbol{f}_T^{(j)}$ of the resulting simplexes $S^{(j)}$ are mapped into the parameter space as $\boldsymbol{x}_T^{(j)} = \boldsymbol{s}_I(\boldsymbol{f}_T^{(j)})$. The vectors $\boldsymbol{x}_T^{(j)}$ are used to determine the domain thickness parameter $T$.

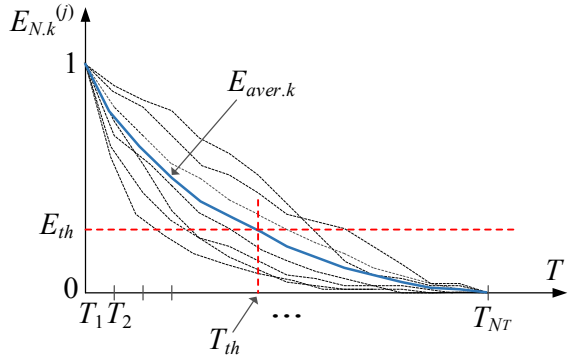


Fig. 5. Exemplary normalized sequences $E_{N.k}^{(j)}$ of (7) and the average sequence $E_{aver.k}$ of (8). The recommended value $T_{th}$ of the thickness parameter corresponds to the threshold value $E_{th}$ of the normalized objective function.

## 4. Numerical Results

This section provides a numerical verification of the procedure for the thickness parameter determination presented in Section 3. Our numerical experiments are conducted for a dual-band dipole antenna and a miniaturized rat-race coupler. In both cases, the objective space is two-dimensional with the figures of interest being the operating frequencies (antenna) and the operating frequency and the power split ratio (coupler). The validation consists of comparing the recommendations obtained using the procedure of Section 3 with the optimization results of the nested kriging surrogates constructed for several values of the thickness parameter.

### 4.1. Case I: Uniplanar Dual-Band Dipole Antenna

The first example is a dual-band uniplanar dipole antenna shown in Fig. 6 [44], implemented on a Rogers RO4350 substrate ($\varepsilon_r$ = 3.5, $h$ = 0.76 mm). It is fed by a 50 Ohm coplanar waveguide (CPW). The structure is described by six geometry parameters $\boldsymbol{x} = [l_1\ l_2\ l_3\ w_1\ w_2\ w_3]^T$, whereas $l_0$ = 30, $w_0$ = 3, $s_0$ = 0.15 and $o$ = 5 are fixed (all dimensions in mm). The EM antenna model $\boldsymbol{R}$ (~100,000 cells; simulation time 60 s) is implemented in CST Microwave Studio and evaluated using its time-domain solver.

We consider two figures of interest being the operating frequencies: $f_1$ for the lower band, and $f_2$ for the upper band. The surrogate model for the antenna is supposed to be constructed over the objective space defined by the following ranges of the mentioned figures: 2.0 GHz ≤ $f_1$ ≤ 3.0 GHz (lower band), and 4.0 GHz ≤ $f_2$ ≤ 5.5 GHz (upper band). The first-level model is rendered using ten reference designs $\boldsymbol{x}^{(j)}$, $j$ = 1, …, 10, corresponding to the following operating frequency pairs: $\{f_1,f_2\}$ = {2.0, 4.0}, {2.2, 5.0}, {2.0, 5.0}, {2.3, 4.5}, {2.4, 5.5}, {2.6, 4.0}, {2.7, 5.3}, {2.8, 4.7}, {3.0, 4.0}, and {3.0, 5.5} (frequencies in GHz). The parameter space $X$ is defined by the lower and upper bounds $\boldsymbol{l}$ = [29 5.0 17 0.2 1.5 0.5]$^T$, and $\boldsymbol{u}$ = [42 12 25 0.6 5.2 3.5]$^T$, derived from $\{\boldsymbol{x}^{(j)}\}$. It is worth noticing that the parameter ranges are

very wide for this case: the ratio between the upper and the lower bounds varies from 1.5 to 7.0 with the average of 3.1. This makes the modeling problem a challenging one.

The procedure of Section 3.2 has been used to estimate a suitable value of the thickness parameter $T$. Figure 7 shows the reference designs, their triangulation, as well as the location of the vectors $\boldsymbol{f}_T^{(j)}$. The problem (6) is solved at $\boldsymbol{x}_T^{(j)} = \boldsymbol{s}_I(\boldsymbol{f}_T^{(j)})$ for the sequence $T_1 = 0.0$, $T_2 = 0.01$, …, $T_{26} = 0.15$. Figure 8 shows the plots of the normalized objective value sequences $E_{N.k}^{(j)}$ as well as the average sequence $E_{aver.k}$. For the threshold level $E_{th} = 0.25$, the recommended value of the thickness parameter is $T_{th} = 0.062$. Here, the objective function values below have been rounded up to 0.03, which corresponds to around –20 dB of the reflection level at and around the antenna resonances. The reason is that, in practice, there is no need to go beyond this value, so that domain extension aimed at further improving the optimization results is not necessary. For this reason, some of the normalized sequences $E_{N.k}^{(j)}$ in Fig. 8 coincide with the horizontal axis because the mentioned objective function value is obtained even for $T = 0$.

Verification of the recommended domain thickness parameter $T_{th}$ has been arranged as follows. The second-level surrogate has been constructed for various thickness parameter values from 0.0 to 0.15 (with the step of 0.01). In each case, 800 training samples were allocated in the corresponding domain $X_S$. Subsequently, the models were optimized for a number of objective vectors $\boldsymbol{f}$, including the points $\boldsymbol{f}_T^{(j)}$, supplemented by a certain number of random locations (50 points in total). Table 1 gathers the numerical data, in particular, the objective function values averaged over the testing set. It can be observed that the average value starts saturating around $T = 0.06$, which agrees very well with $T_{th}$. This indicates that the estimate provided by the procedure of Section 3.2 is indeed reliable.

For additional validation, the models obtained for $T = 0.0$, 0.03, 0.06, and 0.10 have been investigated in more detail, especially to compare the quality (in relation to EM-simulated antenna characteristics) of the optimized designs produced by the respective surrogates. Figure

9 shows the optimized antenna responses obtained for the four considered models and two selected sets of design specifications. It can be observed that the predictions provided by the surrogate agree well with EM simulation results for the models constructed with $T$ = 0.0 through $T$ = 0.06; however, noticeable discrepancies can be observed for $T$ = 0.15. At the same time, as expected, the models constructed in larger domains (i.e., higher values of $T$) allow for yielding design that exhibits improved objective function levels. The recommended value of $T$ = 0.06 seems to be a good compromise between the quality of surrogate prediction and the achievable optimum design. One can also notice that the thickness parameter, which is slightly smaller than the recommended value (here, $T$ = 0.03) may still be considered the right choice. Although the corresponding surrogate is not capable of reducing the objective function as much as the model rendered for $T$ = 0.06, the quality is still comparable, whereas smaller $T$ enables clear computational benefits due to significantly reduced domain volume.

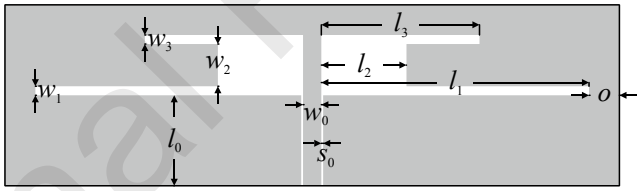


Fig. 6. Geometry of dual-band uniplanar dipole antenna [44].

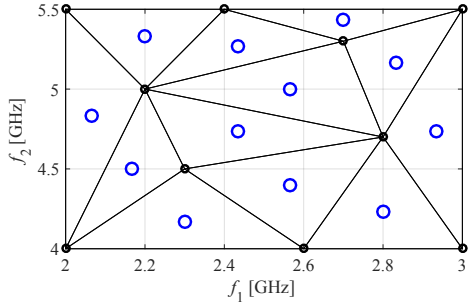


Fig. 7. Dual-band antenna: reference designs (small circles), their triangulation, and the simplex centers (large circles). These points are used as $\boldsymbol{f}_T^{(j)}$ to execute the thickness parameter determination procedure of Section 3.2.

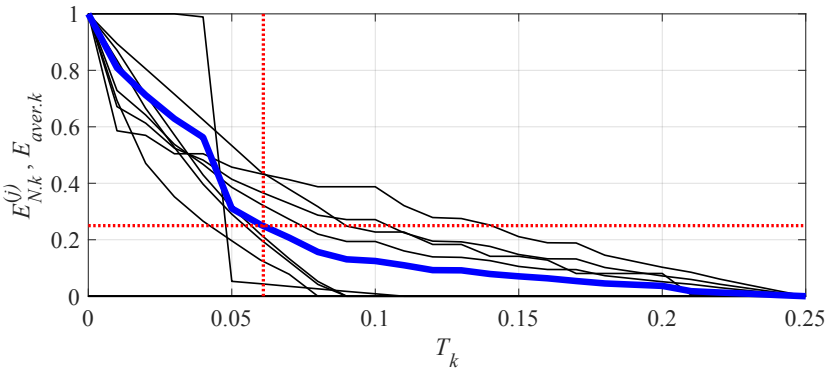


Fig. 8. Dual-band antenna: normalized objective value sequences $E_{N.k}^{(j)}$ (thin lines) and the average sequence $E_{aver.k}$ (thick line). The recommended domain thickness corresponding to the $E_{th}$ = 0.25 is $T_{th}$ = 0.062.

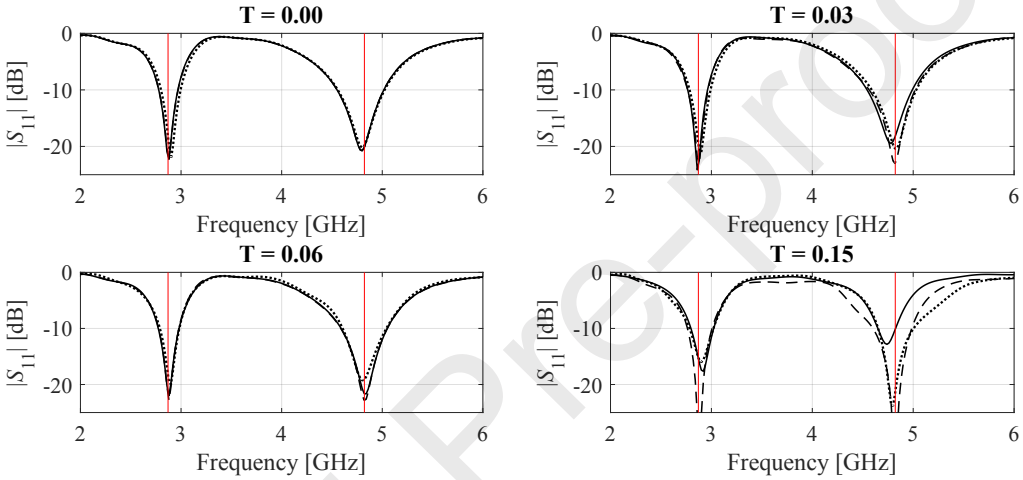


(a)

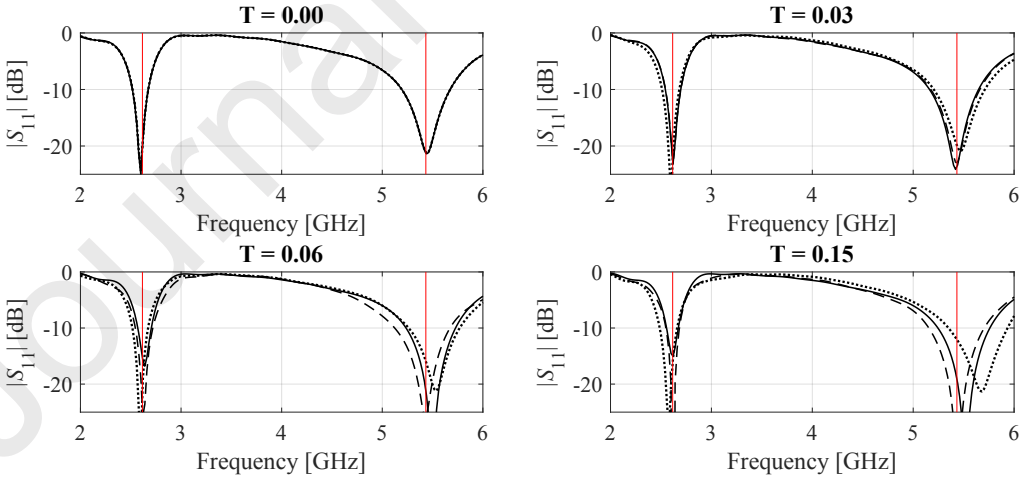


(b)

Fig. 9. Dual-band antenna: initial design (····), surrogate model at the optimized design (- - -), and EM-simulated response at the optimized design (—) for nested-kriging surrogates constructed with the domain thickness parameters $T$ = 0, $T$ = 0.03, $T$ = 0.06 (recommended value), and $T$ = 0.15, shown for two selected target operating frequency vectors ((a), and (b), respectively). The recommended value gives a good compromise between the surrogate model prediction and further agreement with the EM simulation results. The model constructed with smaller $T$ (here, 0.03) can also be considered acceptable, whereas the remaining models either exhibit insufficient coverage of the optimum design manifold ($T$ = 0), or insufficient predictive power of the surrogate ($T$ = 0.15).

Table 1. Dual-band antenna: nested kriging surrogates and their optimization results

| Thickness parameter $T$ | Nested kriging model setup* | Relative RMS error# | Model optimization: average objective function value$ |
|---|---|---|---|
| 0.00 | $N_B$ = 800 | 1.8 % | –15.4 dB |
| 0.01 | $N_B$ = 800 | 1.6 % | –16.9 dB |
| 0.02 | $N_B$ = 800 | 1.9 % | –17.1 dB |
| 0.03 | $N_B$ = 800 | 2.2 % | –17.4 dB |
| 0.04 | $N_B$ = 800 | 2.1 % | –17.5 dB |
| 0.05 | $N_B$ = 800 | 2.4 % | –17.6 dB |
| 0.06 | $N_B$ = 800 | 2.5 % | –17.8 dB |
| 0.07 | $N_B$ = 800 | 3.1 % | –18.0 dB |
| 0.08 | $N_B$ = 800 | 3.1 % | –17.8 dB |
| 0.09 | $N_B$ = 800 | 3.2 % | –17.9 dB |
| 0.10 | $N_B$ = 800 | 3.4 % | –18.2 dB |
| 0.11 | $N_B$ = 800 | 3.5 % | –17.9 dB |
| 0.12 | $N_B$ = 800 | 4.0 % | –18.0 dB |
| 0.13 | $N_B$ = 800 | 4.2 % | –17.8 dB |
| 0.14 | $N_B$ = 800 | 4.6 % | –17.8 dB |
| 0.15 | $N_B$ = 800 | 4.8 % | –18.1 dB |

* $N_B$ stands for the number of training samples. The design of experiments procedure can be found in [41].
# Model accuracy estimated using the split-sample method based on 100 random samples. The table provides relative error $\|\boldsymbol{R}(\boldsymbol{x}) - \boldsymbol{R}_s(\boldsymbol{x})\|/\|\boldsymbol{R}(\boldsymbol{x})\|$ averaged over the testing set.
$ Surrogate model optimized within the domain $X_S$. The displayed value is the average over fifty initial designs including the simplex centers $\boldsymbol{x}_T^{(j)}$ and additional random points.

### 4.2. Case II: Miniaturized Rat-Race Coupler

The second example is a miniaturized rat-race coupler (RRC) [45] shown in Fig. 10. The geometry parameters of the structure are $\boldsymbol{x} = [l_1\ l_2\ l_3\ d\ w\ w_1]^T$; other dimensions are $d_1 = d + |w - w_1|$, $d = 1.0$, $w_0 = 1.7$, and $l_0 = 15$ fixed (all in mm). The transmission lines of the RRC are folded to the inside of the layout in order to reduce its footprint. The structure is implemented on RF-35 substrate ($\varepsilon_r = 3.5$, $h = 0.762$ mm, tan $\delta = 0.0018$). Similarly as for the previous example, the computational model $\boldsymbol{R}$ is also implemented in CST Microwave Studio (here, evaluated using frequency-domain solver).

For the RRC, the figures of interest are the operating frequency $f_0$ and the power split ratio $K$. The goal is to construct the surrogate model covering the objective space defined by the following ranges: 1 GHz to 2 GHz for the operating frequency, and –6 dB do 0 dB (i.e., equal

power split) for $K$. Design optimality for the coupler is understood by fulfilling the following criteria: (i) the transmission characteristics $S_{21}$ and $S_{31}$ realize $|S_{21}| - |S_{31}| = K$ at $f_0$, and (ii) the matching $|S_{11}|$ and isolation $|S_{41}|$ are minimized at $f_0$. In practice, the merit function $U$ is implemented to minimize $|S_{11}|$ and $|S_{41}|$ (as the primary objective) while enforcing $|S_{21}| - |S_{31}| = K$ using the penalty function approach. The first-level surrogate is constructed using twelve reference designs corresponding to the following pairs of $\{f_0,K\}$: {1.0,0}, {1.0,–2}, {1.0,–6}, {1.2,–4}, {1.3,0}, {1.5,–2}, {1.5,–5}, {1.7,0}, {1.7,–6}, {1.8,–3}, {2.0,0}, and {2.0,–6} (frequency in GHz, power split ratio in dB). The lower and upper bounds defining the parameter space $X$ are $\boldsymbol{l} = [2.0\ 7.0\ 12.5\ 0.2\ 0.7\ 0.2]^T$ and $\boldsymbol{u} = [4.5\ 12.5\ 22.0\ 0.65\ 1.5\ 0.9]^T$.

The thickness parameter has been estimated using the procedure of Section 3.2. The reference designs are shown in Fig. 11, along with their triangulation and location of the vectors $\boldsymbol{f}_T^{(j)}$. The problem (6) is solved at $\boldsymbol{x}_T^{(j)} = \boldsymbol{s}_I(\boldsymbol{f}_T^{(j)})$ for the same sequence as in the case of the previous example: $T_1 = 0.0$, $T_2 = 0.01$, …, $T_{26} = 0.15$. Figure 12 shows the normalized objective sequences $E_{N.k}^{(j)}$ and $E_{aver.k}$. Here, the recommended value of the thickness parameter $T_{th}$ is 0.115 (corresponding to the threshold level $E_{th} = 0.25$). The objective function values below have been rounded up to –35 dB which corresponds to good practical designs.

Verification of the recommended value of $T_{th}$ has been realized by constructing and analyzing the second-level surrogate for various thickness parameters from 0.0 to 0.15 (with the step of 0.01). The models were optimized for a number of objective vectors $\boldsymbol{f}$ (the points $\boldsymbol{f}_T^{(j)}$ supplemented by random locations, 50 points in total). Table 2 shows the numerical data, in particular, the objective function values averaged over the testing set. Note that the average value starts saturating around $T = 0.10$, which agrees very well with $T_{th}$. This corroborates the reliability of the estimate provided by the procedure of Section 3.2.

Similarly as in Section 4.1, additional validation has been carried out. The models obtained for $T = 0.0$, 0.06, 0.11, and 0.15 have been investigated in more detail. Figure 13

shows the optimized coupler responses obtained for the considered models. Note that the predictions provided by the surrogate agree well with EM simulation results for the models constructed with $T$ = 0.0 and 0.6, and it is slightly worse for $T$ = 0.11. For $T$ = 0.15, the discrepancies between the surrogate and EM simulation become quite noticeable, i.e., reliability of the optimization process is degraded to a certain extent.

On the other hand, as expected, the models constructed in larger domains (i.e., higher values of $T$) allow for yielding design that exhibits improved objective function levels. Similarly as for the previous example, the recommended value (here, $T$ = 0.11) seems to be a reasonable compromise between the quality of surrogate prediction and the achievable optimum design. Also, using the thickness parameter, which is slightly smaller than the recommended value (here, $T$ = 0.06) seems to be a good option. The surrogate model accuracy is much better for $T$ = 0.06 than for $T$ = 0.11 (4.0 versus 6.6 percent of the average RMS error), whereas the average improvement of the objective function is not significant (less than 1 dB).

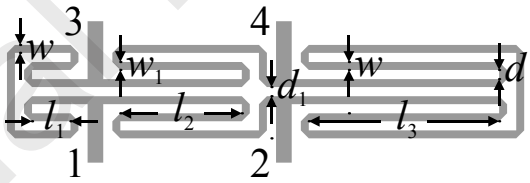


Fig. 10. Geometry of the compact microstrip rat-race coupler (RRC) [45].

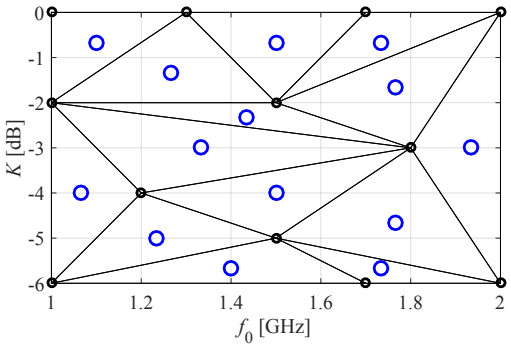


Fig. 11. Rat-race coupler: reference designs (small circles), their triangulation, and the simplex centers (large circles). These points are used as $\boldsymbol{x}_T^{(j)}$ to execute the thickness parameter determination procedure of Section 3.2.

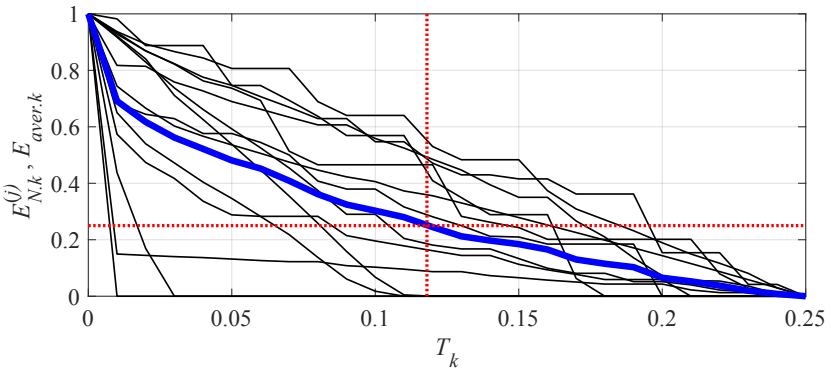


Fig. 12. Rat-race coupler: normalized objective value sequences $E_{N.k}^{(j)}$ (thin lines) and the average sequence $E_{aver.k}$ (thick line). The recommended domain thickness corresponding to the $E_{th}$ = 0.25 is $T_{th}$ = 0.115.

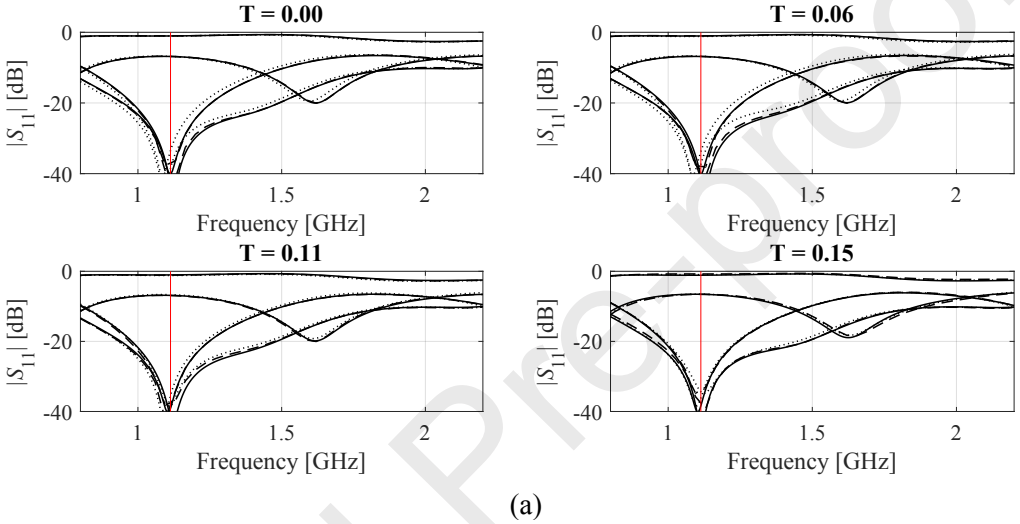


(a)

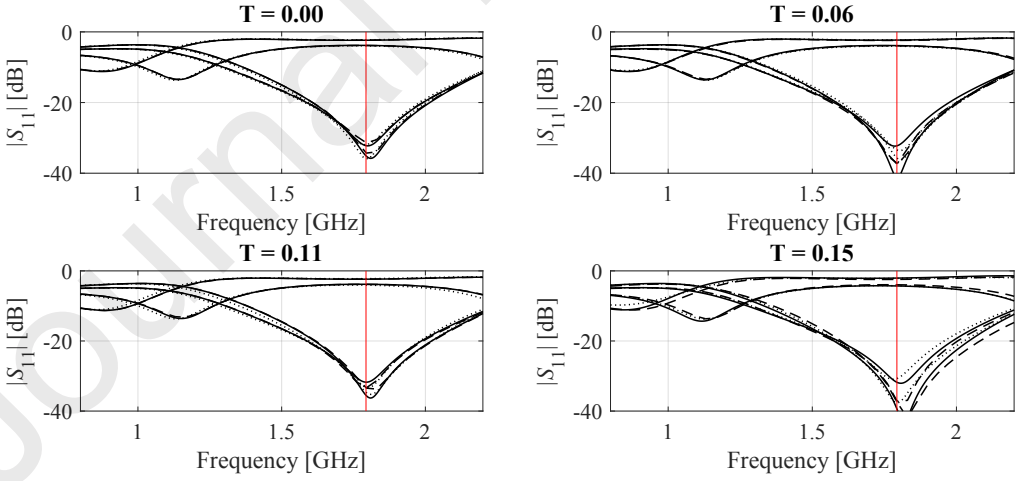


(b)

Fig. 9. Rat-race coupler: initial design (····), surrogate model at the optimized design (- - -), and EM-simulated response at the optimized design (—) for nested-kriging surrogates constructed with the domain thickness parameters $T$ = 0, $T$ = 0.06, $T$ = 0.11 (recommended value), and $T$ = 0.15, shown for two selected target operating frequency vectors ((a), and (b), respectively). The recommended value gives a good compromise between the surrogate model prediction and further agreement with the EM simulation results. The model constructed with smaller $T$ (here, 0.06) can also be considered acceptable. The model with $T$ = 0 shows a somehow limited coverage of the optimum design manifold; however, this effect is here less pronounced than for the first example. The model with $T$ = 0.5 exhibits insufficient predictive power of the surrogate (noticeable discrepancies between the surrogate and EM-simulated responses).

Table 2. Rat-race coupler: nested kriging surrogates and their optimization results

| Thickness parameter $T$ | Nested kriging model setup* | Relative RMS error# | Model optimization: average objective function value$ |
|---|---|---|---|
| 0.00 | $N_B$ = 800 | 0.7 % | –23.8 dB |
| 0.01 | $N_B$ = 800 | 1.2 % | –26.2 dB |
| 0.02 | $N_B$ = 800 | 1.7 % | –26.8 dB |
| 0.03 | $N_B$ = 800 | 2.2 % | –27.3 dB |
| 0.04 | $N_B$ = 800 | 2.8 % | –27.7 dB |
| 0.05 | $N_B$ = 800 | 3.3 % | –28.0 dB |
| 0.06 | $N_B$ = 800 | 4.0 % | –28.1 dB |
| 0.07 | $N_B$ = 800 | 4.6 % | –28.2 dB |
| 0.08 | $N_B$ = 800 | 5.1 % | –28.4 dB |
| 0.09 | $N_B$ = 800 | 5.1 % | –28.6 dB |
| 0.10 | $N_B$ = 800 | 6.1 % | –28.9 dB |
| 0.11 | $N_B$ = 800 | 6.6 % | –29.0 dB |
| 0.12 | $N_B$ = 800 | 7.2 % | –29.0 dB |
| 0.13 | $N_B$ = 800 | 7.7 % | –29.2 dB |
| 0.14 | $N_B$ = 800 | 8.3 % | –29.3 dB |
| 0.15 | $N_B$ = 800 | 8.9 % | –29.3 dB |

* $N_B$ stands for the number of training samples. The design of experiments procedure can be found in [41].
# Model accuracy estimated using the split-sample method based on 100 random samples. The table provides relative error $||\boldsymbol{R}(\boldsymbol{x}) - \boldsymbol{R}_s(\boldsymbol{x})||/||\boldsymbol{R}(\boldsymbol{x})||$ averaged over the testing set.
$ Surrogate model optimized within the domain $X_S$. The displayed value is the average over fifty initial designs including the simplex centers $\boldsymbol{x}_T^{(j)}$ and additional random points.

## 5. Conclusion

The paper proposed a procedure for low-cost a priori determination of the thickness parameter of the surrogate model domain, which is a critical component of setting up the nested kriging framework, the recent approach to constrained modeling of high-frequency structures. The value of this parameter determines the domain volume, which directly translates into a computational cost of training data acquisition, but also the model utility: too small domain hinders applicability of the surrogate in the context of design optimization. So far, the parameter had to be chosen arbitrarily and its relevance could only be assessed a posteriori, upon investigating the properties of the already constructed surrogate. Our methodology allows for reliable domain thickness estimation so that the model domain contains the majority of the

optimum designs (w.r.t. the relevant performance figures and the assumed objective space). The process involves a sequence of constrained optimization runs executed on analytical models (therefore, of negligible cost), with the models themselves constructed using the system responses and their numerical derivatives computed as carefully selected locations. The latter ensures the low cost of the entire scheme. Comprehensive numerical validation involving a dual-band dipole antenna and a miniaturized microstrip coupler demonstrates the relevance of the thickness parameter determination algorithm. The presented procedure is a fundamental component of rendering the nested kriging surrogates, lacking in the original formulation of the method. It permits an adequate establishment of the region of validity of the model and allows for maximizing its utility while retaining the practically acceptable cost of training data acquisition.

## Acknowledgement

The authors would like to thank Dassault Systemes, France, for making CST Microwave Studio available. This work is partially supported by the Icelandic Centre for Research (RANNIS) Grant 174114051 and by National Science Centre of Poland Grant 2018/31/B/ST7/02369.

## References

[1] A. Contreras, M. Ribo, L. Pradell, V. Raynal, I. Moreno, M. Combes, and M. Ten, "Compact fully uniplanar bandstop filter based on slow-wave multimodal CPW resonators," *IEEE Microwave Wireless Comp. Lett.*, vol. 28, no. 9, pp. 780-782, 2018.

[2] C.H. Tseng and C.L. Chang, "A rigorous design methodology for compact planar branch-line and rat-race couplers with asymmetrical T-structures," *IEEE Trans. Microw. Theory Techn.*, vol. 60, no. 7, pp. 2085–2092, 2012.

[3] M. Naderi, F.B. Zarrabi, F.S. Jafari, S. Ebrahimi, "Fractal EBG structure for shielding and reducing the mutual coupling in microstrip patch antenna array," *AEU - Int. J. Electr. Comm.*, vol. 93, pp. 261-267, 2018.

[4] S. Kim and S. Nam, "A compact and wideband linear array antenna with low mutual coupling," *IEEE Trans. Ant. Prop.*, vol. 67, no. 8, pp. 5695-5699, 2019.

[5] T. Anilkumar, B.T.P. Madhav, M. Venkateswara Rao, B. Prudhvi Nadh, "Bandwidth reconfigurable antenna on a liquid crystal polymer substrate for automotive communication applications," *AEU - Int. J. Electr. Comm.*, vol. 117, art. no. 153096, 2020.

[6] T.A. Elwi, H.M. Al-Rizzo, D.G. Rucker, H.R. Khaleel, "Effects of twisting and bending on the performance of a miniaturized truncated sinusoidal printed circuit antenna for wearable biomedical telemetry devices," *AEU - Int. J. Electr. Comm.*, vol. 65, no. 3, pp. 217-225, 2011.

[7] P. Martin-Iglesias, T. Raadik, F. Teberio, J.M. Percaz, S. Martin-Iglesias, L. Pambaguian, I. Arregui, I. Arnedo, T. Lopetegui, and M.A.G. Laso, „Multiphysic analysis of high power microwave filter using high performance alluminium alloy," *IEEE MTT-S Int. Microwave Workshop Series on Advanced Materials and Processes for RF and THz Applications (IMWS-AMP)*, Bochum, Germany, 16-18 July, 2019.

[8] H. Malhi and M.H. Bakr, "Geometry evolution of microwave filters exploiting self-adjoint sensitivity analysis," *Int. Conf. Numerical Electromagnetics and Multiphysics Mod. Opt. (NEMO)*, Ottawa, Canada, 11-14 Aug. 2015.

[9] D.I. Karatzidis, T.V. Yioultsis, T.D. Tsiboukis, "Gradient-based adjoint-variable optimization of broadband microstrip antennas with mixed-order prism macroelements," *AEU - Int. J. Electr. Comm.*, vol. 62, no. 6, pp. 401-412, 2008.

[10] S. Koziel, S. Ogurtsov, Q.S. Cheng, and J.W. Bandler, "Rapid EM-based microwave design optimization exploiting shape-preserving response prediction and adjoint sensitivities," *IET Microwaves, Ant. Prop.*, vol., 8, no. 10, pp. 775-781, 2014.

[11] S. Koziel and A. Pietrenko-Dabrowska, "Variable-fidelity simulation models and sparse gradient updates for cost-efficient optimization of compact antenna input characteristics," *Sensors*, vol. 19, no. 8, 2019.

[12] S. Koziel and A. Pietrenko-Dabrowska, "Reduced-cost electromagnetic-driven optimization of antenna structures by means of trust-region gradient-search with sparse Jacobian updates," *IET Microwaves Ant. Prop.*, vol. 13, no. 10, pp. 1646-1652, 2019.

[13] J.A. Easum, J. Nagar, P.L. Werner, and D.H. Werner, "Efficient multi-objective antenna optimization with tolerance analysis through the use of surrogate models," *IEEE Trans. Ant. Prop.*, vol. 66, no. 12, pp. 6706-6715, 2018.

[14] A.K.S.O. Hassan, A.S. Etman, and E.A. Soliman, "Optimization of a novel nano antenna with two radiation modes using kriging surrogate models," *IEEE Photonic J.*, vol. 10, no. 4, art. no. 4800807, 2018.

[15] R. Kumar, P. Kumar, S. Singh, R. Vijay, "Fast and accurate synthesis of frequency reconfigurable slot antenna using back propagation network," *AEU - Int. J. Electr. Comm.*, vol. 112, art. no. 152962, 2019.

[16] J. Zhang, C. Zhang, F. Feng, W. Zhang, J. Ma, and Q.J. Zhang, "Polynomial chaos-based approach to yield-driven EM optimization," *IEEE Trans. Microwave Theory Tech.*, vol. 66, no. 7, pp. 3186-3199, 2018.

[17] J.W. Bandler, Q.S. Cheng, S.A. Dakroury, A.S. Mohamed, M.H. Bakr, K. Madsen, and J. Søndergaard, "Space mapping: the state of the art," *IEEE Trans. Microwave Theory Tech.*, vol. 52, no. 1, pp. 337-361, Jan. 2004.

[18] S. Koziel and S. Ogurtsov, "Antenna design by simulation-driven optimization. Surrogate-based approach," Springer, 2014.

[19] P. Kurgan, S. Koziel, "Selection of circuit geometry for miniaturized microwave components based on concurrent optimization of performance and layout area," *AEU - Int. J. Electr. Comm.*, vol. 108, pp. 287-294, 2019.

[20] S. Koziel, "Fast simulation-driven antenna design using response-feature surrogates," *Int. J. RF & Micr. CAE*, vol. 25, no. 5, pp. 394-402, 2015.

[21] S. Koziel and L. Leifsson, "Simulation-driven design by knowledge-based response correction techniques," Springer, 2016.

[22] A.M. Alzahed, S.M. Mikki, and Y.M.M. Antar, "Nonlinear mutual coupling compensation operator design using anovel electromagnetic machine learning paradigm," *IEEE Ant. Wireless Prop. Lett.*, vol. 18, no. 5, pp. 861-865, 2019.

[23] J. Tak, A. Kantemur, Y. Sharma, and H. Xin, "A 3-D-printed W-band slotted waveguide array antenna optimized using machine learning," *IEEE Ant. Wireless Prop. Lett.*, vol. 17, no. 11, pp. 2008-2012, 2018.

[24] H.M. Torun and M. Swaminathan, "High-dimensional global optimization method for high-frequency electronic design," *IEEE Trans. Microwave Theory Techn.*, vol. 67, no. 6, pp. 2128-2142, 2019.

[25] J. Du and C. Roblin, "Stochastic surrogate models of deformable antennas based on vector spherical harmonics and polynomial chaos expensions: application to textile antennas," *IEEE Trans. Ant. Prop.*, vol. 66, no. 7, pp. 3610-3622 , 2018.

[26] A. Petrocchi, A. Kaintura, G. Avolio, D. Spina, T. Dhaene, A. Raffo, and D.M.P.-P. Schreurs, „Measurement uncertainty propagation in transistor model parameters via polynomial chaos expansion," *IEEE Microwave Wireless Comp. Lett.*, vol. 27, no. 6, pp. 572-574, 2017.

[27] D. Gorissen, K. Crombecq, I. Couckuyt, T. Dhaene, and P. Demeester, „A surrogate modeling and adaptive sampling toolbox for computer based design," *J. Machine Learning Research*, vol. 11, pp. 2051-2055, 2010.

[28] S. Marelli and B. Sudret, „UQLab: a framework for uncertainty quantification in Matlab," in *The 2nd Int. Conf. on Vulnerability and Risk Analysis and Management (ICVRAM 2014)*, University of London, UK, July 13-15, pp. 2554-2563, 2014.

[29] P. Barmuta, F. Ferranti, G.P. Gibiino, A. Lewandowski and D.M.M.P. Schreurs, "Compact behavioral models of nonlinear active devices using response surface methodology," *IEEE Trans. Microwave Theory and Tech.,* vol. 63, no. 1, pp. 56-64, 2015.

[30] N.V. Queipo, R.T. Haftka, W. Shyy, T. Goel, R. Vaidynathan, and P.K. Tucker, "Surrogate-based analysis and optimization," *Progress in Aerospace Sciences*, vol. 41, no. 1, pp. 1-28, 2005.

[31] J. Dong, W. Qin, and M. Wang, "Fast multi-objective optimization of multi-parameter antenna structures based on improved BPNN surrogate model," *IEEE Access*, vol. 7, pp. 77692-77701, 2019.

[32] J. Cai, J. King, C. Yu, J. Liu and L. Sun, "Support vector regression-based behavioral modeling technique for RF power transistors," *IEEE Microwave and Wireless Comp. Lett.,* vol. 28, no. 5, pp. 428-430, 2018.

[33] J.P. Jacobs, "Characterization by Gaussian processes of finite substrate size effects on gain patterns of microstrip antennas," *IET Microwaves Ant. Prop.*, vol. 10, no. 11, pp. 1189-1195, 2016.

[34] A.C. Yücel, H. Bağcı, and E. Michielssen, "An ME-PC enhanced HDMR method for efficient statistical analysis of multiconductor transmission line networks," *IEEE Trans. Comp. Packaging and Manufacturing Techn.*, vol .5, no. 5, pp. 685-696, 2015.

[35] X. Li, "Finding deterministic solution from underdetermined equation: large-scale performance modeling of analog/RF circuits," *IEEE Trans. on Computer-Aided Design of Integrated Circuits and Systems* (*TCAD*), vol. 29, no. 11, pp. 1661-1668, 2010.

[36] R. Hu, V. Monebhurrun, R. Himeno, H. Yokota, and F. Costen, „An adaptive least angle regression method for uncertainty quantification in FDTD computation," *IEEE Trans. Ant. Prop.*, vol. 66, no. 12, pp. 7188-7197, 2018.

[37] M.C. Kennedy and A. O'Hagan, "Predicting the output from complex computer code when fast approximations are available", *Biometrika,* vol. 87, pp. 1-13, 2000.

[38] F. Wang, P. Cachecho, W. Zhang, S. Sun, X. Li, R. Kanj and C. Gu, "Bayesian model fusion: large-scale performance modeling of analog and mixed-signal circuits by reusing early-stage data," *IEEE Trans. on Computer-Aided Design of Integrated Circuits and Systems (TCAD)*, vol. 35, no. 8, pp. 1255-1268, 2016.

[39] S. Koziel, "Low-cost data-driven surrogate modeling of antenna structures by constrained sampling," *IEEE Antennas Wireless Prop. Lett.*, vol. 16, pp. 461-464, 2017.

[40] S. Koziel and A.T. Sigurdsson, "Triangulation-based constrained surrogate modeling of antennas," *IEEE Trans. Ant. Prop.*, vol. 66, no. 8, pp. 4170-4179, 2018.

[41] S. Koziel and A. Pietrenko-Dabrowska, "Performance-based nested surrogate modeling of antenna input characteristics," *IEEE Trans. Ant. Prop.*, vol. 67, no. 5, pp. 2904-2912, 2019.

[42] S. Koziel and A. Pietrenko-Dabrowska, "Reduced-cost surrogate modeling of compact microwave components by two-level kriging interpolation," *Eng. Opt.*, 2019.

[43] H. Borouchaki, P.L. George, and S.H. Lo, "Optimal Delaunay point insertion," *Int. J. Numerical Methods in Engineering*, vol. 39, no. 20, pp. 3407-3437, 1996.

[44] Y.-C. Chen, S.-Y. Chen, and P. Hsu, "Dual-band slot dipole antenna fed by a coplanar waveguide," *IEEE Int. Symp. Ant. Prop.*, pp. 3589-3592, 2006.

[45] S. Koziel, A. Bekasiewicz, P. Kurgan, and J.W. Bandler, "Expedited multi-objective design optimization of miniaturized microwave structures using physics-based surrogates," *IEEE MTT-S Int. Microwave Symp.*, pp. 1-3, 2015.